miR-144-3p Regulates Vascular Smooth Muscle Cell Phenotypic Switch via FBN1

Aiqi Lin
Huashan Hospital Fudan University
Xiaocui Kang
Fifth People's Hospital of Shanghai Fudan University
Yuqiong Jiao
Huadong Hospital Affiliated to Fudan University
Xiaochao Feng
Fifth People's Hospital of Shanghai Fudan University
Yi Xu
Huashan Hospital Fudan University
Wei Yan
Huashan Hospital Fudan University
Yao Li
Huashan Hospital Fudan University
Xiang Han (hansletter@fudan.edu.cn)
Huashan Hospital Fudan University https://orcid.org/0000-0003-4608-2083
Qiang Dong
Huashan Hospital Fudan University

Research Article

Keywords: Carotid artery dissection (CAD), FBN1, microRNA-144-3p, vascular smooth muscle cell

Posted Date: November 3rd, 2021

DOI: https://doi.org/10.21203/rs.3.rs-953523/v1

Abstract

Background: Carotid artery dissection (CAD) represents a commonly reported factor causing stroke in young and middle-aged adults. Vascular wall remodeling is one of its important pathogenetic mechanisms. FBN1 is a common pathogenic gene leading to Marfan syndrome, whose mutation can cause the formation of aneurysm and arterial dissection. It was recently demonstrated multiple miRNAs contribute to the development of arterial dissection, while miR-144-3p's function is undefined.

Methods: In the current study, vascular smooth muscle cells (VSMCs) were transfected with miR-144-3p mimic and inhibitor, as well as siFBN1 and miR-144-3p + siFBN1, to determine vascular smooth muscle's contractile genes, extracellular matrix-associated proteins. In addition, miR-144-3p's effects on cell proliferation, migration, adhesion, invasion and apoptosis were evaluated.

Results: The results revealed miR-144-3p had elevated amounts, while the fibrillin-1 protein showed reduced expression in arterial dissection tissues. Meanwhile, FBN1 was shown to be a miR-144-3p target by dual-luciferase gene reporter assay. In response to miR-144-3p mimic transfection, decreased expression of VSMC contractile gene markers, increased apoptosis, and decreased proliferation, migration, and invasion were found.

Conclusions: Overall, miR-144-3p affects the biological function of VSMCs by targeting and regulating FBN1, decreases the expression of contractile genes，transforms the phenotype and leads to vascular wall remodeling.

Introduction

Carotid artery dissection (CAD) represents a frequent factor causing stroke in young and middle-aged adults. Studies have found that 10–25% of patients aged 19 to 45 years with first-episode stroke have undergone arterial dissection [1]. Dissection of the arterial wall, due to a tear in the artery's intimal layer or arterial wall bleeding, can be serious and life-threatening. Although the exact pathogenetic mechanism of arterial dissection remains uncertain, vascular smooth muscle cells (VSMC), as the major constituent of the arterial wall media, are currently considered the main cells leading to arterial dissection formation. [2, 3]

Fibrillin-1, a product of the FBN1 gene, is a 2871 amino-acid glycoprotein with a molecular weight of 350 kDa, and the microfiber component containing it is the backbone of elastic fibers in the vessel wall, which, together with other extracellular matrix proteins, determines the mechanical stability and histophysical properties of the extracellular matrix. [4] The FBN1 gene is an important pathogenic gene in Marfan syndrome, and consists of 65 exons. The RGD sequence of the TB4 domain of the fibrillin-1 protein encoded by this gene can bind to a variety of integrin receptors, which in turn are involved in cytoskeletal regulation, affecting vascular smooth muscle function and extracellular matrix homeostasis. When fibrillin-1 protein content in the vascular wall is reduced, extracellular matrix stability is affected and intercellular adhesion is decreased, which can cause morphological remodeling and phenotypic changes

in vascular smooth muscle cells (VSMC). [5] Although previous studies have found that arterial dissection can be largely attributed to polymorphic defects in the FBN1 gene, other disruptive factors, such as fibrillin-1 protein amounts and translational regulation, might also have an important function in arterial dissection's pathogenesis.

MicroRNAs (miRNAs) are non-coding RNAs of about 20 ~ 22 nucleotides in length. They are also the shortest eukaryotic RNAs. [6] Most miRNAs bind via the 3' UTR regions of their respective target genes, although also binding sites in the 5' -UTR or exosome regions. [7] Upon binding, the target gene is silenced due to changes in spatial structure. MicroRNAs have critical functions in multiple biomolecular processes, including cell differentiation, cell identity determination, apoptosis, cell migration and cell cycle. [8–11] Of reported miRNAs, miR-144-3p has been broadly examined. Indeed, miR-144-3p targets have been published, e.g., E26 transformation specific-1, [12] cyclooxygenase-2, [13] adenosine triphosphate-binding cassette transporter, [14] and cyclin-dependent kinase inhibitor 2D. [15] Nevertheless, whether miR-144-3p targets the FBN1 gene is unknown.

Here, miR-144-3p's effect on fibrillin-1 protein levels in VSMC through regulation of FBN1 was examined. This study indicated miR-144-3p targets the FBN1 gene in both humans and rats. Bioinformatic analysis and dual-luciferase reporter assay demonstrated miR-144-3p downregulated FBN1 at the gene and protein levels by interacting with the 3' -UTR of FBN1 mRNA. Additionally, in the animal model, higher miR-144-3p levels and lower fibrillin-1 were detected in carotid artery specimens on the modeling side compared with the control side. Transfection of vascular smooth muscle cells with miR-144-3p mimics reduced both FBN1 mRNA and protein amounts, altering the levels of contractile genes, extracellular matrix genes, and matrix metalloproteinases associated with smooth muscle cell phenotype. Cell proliferation, scratch and adhesion assays also revealed miR-144-3p suppressed migration, proliferation, and adhesion in vascular smooth muscle, but promoted apoptosis.

Methods

Modeling

Male SD rats (4 W, 60-80 g), provided by Shanghai Jasper Laboratory Animal Co., Ltd. and housed under specific pathogen-free (SPF) conditions, received standard chow, with free access to water. They were randomly divided into the normal group (drinking tap water, n=8) and model animals (n=8), which were administered β-aminopropionitrile monofumarate (BAPN, Sigma, USA) in drinking water at 0.4 g/100 g diet for 28 days as previously proposed. [16]

Establishment of the animal model of carotid artery dissection

(a) Anesthesia: Before sampling, the animals were fasted for 4 hours and intraperitoneally administered pentobarbital sodium (3 ml/Kg body weight) for anesthesia. The experimental design and anesthesia had approval from the Animal Room Ethics Committee of Fudan University.

(b) Modeling: After local disinfection of the neck, the neck's skin along the midline was longitudinally incised, and the left and right carotid arteries were carefully separated. A carotid artery was randomly selected, and two small edentulous microhemostatic clips were used to clamp the carotid artery from both sides of the head and tail in the opposite direction of the handle end (the distance between the two hemostatic clips was 1 cm). Then, both hemostatic clips were rotated at 180° in the opposite direction and fixed (Figure 2A); the other internal carotid artery was left untreated and used as a control.

(c) Specimen collection and storage: After 20 min, the microvascular clamp was gently removed, and the skin was sutured and disinfected. Carotid arteries were taken 24 hours later for subsequent experiments.

(d)All rats dying before the expected study end time (4 weeks) were necropsied right away.

Animal experiments were performed at the Institute of Neurology, Huashan Hospital, Fudan University. The animal experiments followed the Guide for the Care and Use of Laboratory Animals, and had approval from the Institutional Animal Care and Use Committee of Huashan Hospital, Fudan University.

Cell culture, grouping and transfection

A7R5 smooth muscle cells (SMC), provided by Shanghai Cell Bank, Chinese Academy of Sciences, were maintained in Dulbecco's modified Eagle's medium (DMEM, 190040; Gibco) with 10% fetal bovine serum (FBS) in a 5% CO_2 incubator at 37°C. Cells were then seeded in 6-well plates at 10^5/well and underwent incubation at 37°C in a 5% CO_2 incubator, with the medium refreshed at 2 to 3-day intervals. At 70-80% confluency, cell sub-culturing was carried out. This was followed by two PBS washes, a 1-2-minute incubation with 0.25% trypsin, and resuspension and subculture in DMEM with 10% FBS.

Actively growing A7R5 SMC were assigned to blank (A7R5 SMC; transfection with no sequence), negative control (NC), miR-144-3p mimic(transfection with miR-144-3p mimic),miR-144-3p inhibitor (transfection with miR-144-3p inhibitor),siRNA-FBN1(transfection with siRNA-FBN1)and miR-144-3p inhibitor + siRNA-FBN1 (co-transfection with miR-144-3p inhibitor and siRNA-FBN1) groups, respectively. Transfection was carried out on 6-well plates using the RNAimax reagent (Invitrogen, USA) as directed by the manufacturer at 70% to 80% confluency. The miR-144-3p mimic, siRNA-FBN1, miR-144-3p inhibitor, miR-144-3p inhibitor+siRNA-FBN1 and NC were from Genepharma Gene Co., Ltd. (Shanghai, China), and RNase-free water was utilized for solubilization.

Next, 250 μL of Opti-MEM (Gibco) without serum was added to 5 μL of RNAimax reagent and incubated for 5 min at ambient. The two abovementioned solutions were added to cell culture wells following a 20-minute incubation at ambient. After 6-8 hours of culture at 37°C in 5% CO_2 incubator, the medium was changed to complete medium for further culture for 24-48 hours. A fluorescence microscope (Wanheng Precision Instrument, Shanghai, China) was used for analysis. RNA and protein extractions from cells were carried out for subsequent assays.

Hematoxylin - eosin staining and EVG staining

Carotid artery tissue specimens from normal animals and carotid artery dissection tissue samples from model animals were collected. Upon fixation with 4% formalin for 24 h, the tissue specimens underwent dehydration with graded ethanol and N-butanol and paraffin embedding at 60°C, followed by 5-μm serial sectioning. Dewaxing was carried out at 60°C for 1 h with xylene.

For H&E staining, incubation was first performed with hematoxylin (3–5 min). After incubation with acid and ammonia solutions for 40 s each, the samples underwent staining with eosin (2 min) and were soaked in xylene (5 min). An inverted microscope (Olympus, Tokyo, Japan) was utilized for analysis.

In EVG staining, a 30-min incubation was carried out with EVG solution (hematoxylin, iodine solution and ferric chloride at 5:2:2) followed by washing. Ferric chloride differentiation solution was utilized for background. These steps were repeated until a grey white background was obtained. This was followed by staining with VG solution (saturated picric acid and Fuchsin solution at 9:1), multiple washes and dehydration with 100% ethanol. After neutral gum sealing, an inverted microscope (Olympus) was utilized for analysis.

Immunohistochemistry

Carotid artery tissue specimens from normal animals and carotid artery dissection tissue samples from model animals underwent fixation with 10% formalin, paraffin embedding and sectioning 3-4 μm. After treatment with 3% H_2O_2, xylene dewaxing (10 min) and dehydration with graded ethanol were performed. This was followed by antigen retrieval by boiling for 90 seconds. The samples were blocked with 5% bovine serum albumin for 30 min at 37°C, followed by incubation with rabbit anti-rat FBN1 antibodies (ab523076, Abcam; 1:300) overnight at 4°C. Next, the specimens underwent incubation with horseradish peroxidase (HRP)-linked goat anti-rabbit IgG-secondary antibodies (ab6721, Abcam) for 30 min at 37°C. The sections were counterstained with hematoxylin for 30 s and developed with diaminobenzidine (P0202; Beyotime Biotechnology). Next, hydrochloric acid solution was utilized for dehydration, which was followed by mounting with neutral balsam and microscopic analysis. In this study, positivity was considered as >25% cells stained for fibrillin-1 (brown or tan granules in the cytosol). Totally five high-power visual fields (40×) were randomly examined, and 200 cells were enumerated per field. Positive cells per field were counted and averaged.

Reverse transcription quantitative polymerase chain reaction (Table. 1)

Immunoblot

Normal carotid tissue and carotid tissue samples (200 mg) were homogenized and stored at -80ºC. In *in vitro* assays, cells underwent 2 washes with PBS containing protein lysis buffer, followed by centrifugation for 20 min at 4°C and 12000g for protein extraction. The resulting supernatant was treated with the bicinchoninic acid Protein Assay Kit (P0012-1; Beyotime). Equal amounts of total protein (20 μg) were resolved by 10% sodium dodecyl sulfate (SDS)-polyacrylamide gel electrophoresis (PAGE), followed by electro-transfer onto polyvinylidene fluoride (PVDF) membranes. Upon 1-h of blocking at ambient with

5% fat-free milk, the membranes underwent incubation with rabbit anti-Rat FBN1 (ab231094,1:500), MYH11 (ab125884,1:3000), CNN1 (ab32124, 1:1000), ACTA2 (ab7817,1:3000), MMP2 (ab92536, 1:1000), MMP9 (ab76003, 1:1000), ELN (ab21610, 1:1000), COL1A1(ab34710, 1:1000) and GAPDH (ab8245, 1:3000) primary antibodies (Abcam). This was followed by incubation with Tris Buffered Saline-Tween (TBS-T). The enhanced chemiluminescence kit was utilized for detection by autoradiography. Optical density (OD) was obtained with a gel detection system, normalized to GAPDH. The assays were repeated thrice.

Dual - luciferase reporter gene assay

The luciferase reporter assay identifies target miRNAs of the rat and human FBN1 genes via the TargetScan database, scoring them with the context + + scoring system of the database. [17] Dual-luciferase reporter plasmids p3'-UTR-FBN1 (comprising the wild-type FBN13'-UTR binding site in the luciferase reporter plasmid) and p3'-UTR-FBN1mut (comprising the mutant FBN1 3'-UTR; mut), miR144-3p mimic, miR-144-3p inhibitor and negative control (NC) sequences were constructed by Shanghai Hanheng Biotechnology. For luciferase assays, the completed 3'-UTR plasmids underwent co-transfection with miR144-3p mimic, miR-144-3p inhibitor, and negative control (NC) sequences into HEK-293T cells with Lipofectamine 3000 reagent (Invitrogen, Shanghai China) for 48 h. The Dual-Luciferase Reporter Assay System (Promega, China) was utilized for Luciferase activity measurement as directed by the manufacturer.

Proliferation Assay

Approximately 10^4 cells were seeded in 96-well plates for 24 h, and underwent transfection with miR-144-3p mimic, miR-144-inhibitor, negative control (NC), siFBN1 and miR-144-3p+siFBN1 for 24 h and further incubation with medium with 0.5% FBS for 48 h. After treatment, 10 µl CCK-8 was supplemented to the culture medium for 2.5 h. At the 2.5, 24, 48 and 72-h time points, respectively, OD at 450 nm was obtained on a Synergy H1 Bio TEK (Ptotem Instruments Co., Ltd. USA).

Migration assay

Upon transfection for 24 h, cells were seeded in 6-well plates at 5×10^5/well. At 90% confluency, a 200-µl tip was utilized for scratching, which was followed by a PBS wash. Serum-free medium was next supplemented for another 0.5-1 h. At 0 h, 24 h and 48 h, respectively, cell imaging was performed, followed by migration distance measurement with Image-Pro Plus Analysis (Media Cybernetics, MD). Assays were performed three times.

Cell Adhesion Assessment

Totally 50 mg/L Matrigel (356234; BD Diagnostics) was diluted 1:10 with FBS-free culture medium, and 60 µl/well was used to coat 96-well plates, followed by incubation in a 37°C/5% CO_2 incubator for 4 hours. The supernatant was aspirated and discarded. Then, the transfected cells underwent seeding in

96-well plates at 5×10^4/well, with 5 duplicate wells per group. Meanwhile, a control group was set up, that is, a group with the supernatant not discarded after incubation. After 4 h, the culture medium was aspirated, and non-adherent cells were washed off. Totally 100 μl of fresh medium was added to each well, and 5 μl of CCK8 solution was added to each well for incubation in the dark. In the control group, 5 μl of CCK8 was directly added (counted as 0 h). After 4 hours of culture (counted as 4 h), OD at 450 nm was obtained on a Synergy H1 BioTEK (Ptotem Instruments Co., Ltd. USA).

Transwell assay

Matrigel (356234; BD Diagnostics) diluted with serum-free medium at 1:3 was used to coat the upper transwell chambers (50 μL/well) for 30 min at 37ºC. Totally, 10^5 cells/ml were added to upper chambers in medium without serum, while 10% FBS-containing medium was placed into lower chambers. Based on the amounts of cells passing through the matrigel, cell invasion was quantitated. The assays were run thrice.

Statistical analysis

SPSS 22.0 and GraphPad Prism 8 were utilized for data analysis. Data are mean ± standard deviation (SD). The t test and one-way analysis of variance were performed to assess group pairs and multiple groups, respectively. $P<0.05$ reflected statistical significance.

Results

Pathological alterations of vessel wall tissues after dissection

An animal model of spontaneous arterial dissection was established with mechanical clip rotation as previously described (Figure 1A). H&E staining showed that compared with the carotid artery tissue of completely normal animals and the carotid artery tissues of the non-rotation side of model animals, the carotid artery tissue of the rotation side was disorganized and disordered, accompanied by surrounding inflammatory cell infiltration. EVG elastic fiber staining showed disorganized, disordered tissue, and multiple breaks in the elastic fiber component in the arterial dissection tissue (Figure 1B and 1C).

Fibrillin-1 protein expression is lower in the tissues of arterial dissection

After immunohistochemical staining (Figure 2A and 2B), the stained artery dissection tissues had a lighter color with reduced amounts of tan particles. Meanwhile, the normal tissues were dark upon staining, with overtly more than particles in comparison with the artery dissection tissue. In comparison with normal tissues, the positivity rate of fibrillin-1 was higher in the artery dissection tissues ($P<0.05$).

Elevated miR-144-3p expression, reduced FBN1 and extracellular matrix protein amounts, and enhanced MMPs expression in arterial dissection tissues.

Based on RT-qPCR (Figure 3A) and immunoblot (Figure 3B and 3C) findings, arterial dissection tissue samples had increased miR-144-3p levels, and decreased amounts of FBN1, MYH11, ACTA2, CNN1, SRF, MMP2, MMP9, ELN and COL1A1, compared with normal vascular tissue specimens (all $P<0.05$).

FBN1 is a miR-144-3p target

Online analysis demonstrated miR144-3p's binding sites at the 3'-UTRs of human and rat FBN1 mRNAs were from 2611 to 2617 (Figure 4A) and 2585 to 2591 base pairs (Figure 4B), respectively. After comparison, the binding sequences were very similar in human and rat species. Therefore, this study in the rat model might be applied to humans.

To assess whether miR-144-3p's interaction with FBN1 mRNA indeed suppresses FBN1 mRNA expression, the wild-type 3'-UTR of FBN1mRNA (FBN13'-UTR) and the counterpart mutated at the miR-144-3p's binding site (FBN13'-UTRmut) were cloned into luciferase reporter plasmids, respectively. Then, in HEK-293T cells, miR-144-3p/Negative Control (NC) and the FBN1 3'-UTR or FBN1 3'-UTRmut plasmids were co-transfected and examined by dual luciferase reporter assays (Figure 4C). The results showed miR-144-3p significantly reduced luciferase activity in FBN1-3'UTR-WT in comparison with the NC group ($P<0.001$), while miR-144-3p failed to decrease luciferase activity in FBN1-3'UTR-MUT ($P>0.05$) (Figure 4D). Additionally, inhibition of miR-144-3p levels increased fibrillin-1 protein expression in HEK-293T cells, while elevated miR-144-3p suppressed fibrillin-1 protein expression. The above results confirmed that the FBN1 gene is a miR-144-3p target.

MiR-144-3p overexpression decreases FBN1 gene expression and alters the expression of extracellular matrix genes, vascular smooth muscle cell contractile genes and MMPs

The amounts of miR-144-3p, MMP2 and MMP9 were overtly increased, while FBN1, MYH11, ACTA2, CNN1, SRF, ELN and COL1A1 mRNA and protein amounts were reduced in the groups in comparison with the blank group (all $P<0.05$, Figure 5). Compared with the blank and NC groups, miR-144-3p, MMP2 and MMP9 amounts were remarkably elevated in the miR-144-3p mimic group ($P<0.05$); meanwhile, the miR-144-3p mimic and siRNA-FBN1 groups had reduced mRNA and protein amounts of FBN1, MYH11, ACTA2, CNN1, SRF, ELN and COL1A1 (all $P<0.05$). The miR-144-3p inhibitor group had reduced miR-144-3p amounts, and elevated FBN1, MYH11, ACTA2, CNN1, SRF, ELN and COL1A1 mRNA and protein amounts (all $p<0.05$). Finally, the miR-144-3p inhibitor + siRNA-FBN1 group showed decreased miR-144-3p amounts ($P<0.05$), and FBN1, MYH11, ACTA2, CNN1, SRF, ELN and COL1A1 mRNA and protein amounts were elevated (all $p<0.05$).

Upregulated miR-144-3p or downregulated FBN1 inhibits smooth muscle cell proliferation

The CCK8 assay showed that cell proliferation ability in the other four groups was significantly changed after 48 h compared with the blank and NC group (all $P<0.05$). In comparison with the blank and NC group, cell proliferation in the miR-144-3p mimic and siRNA-FBN1 groups was reduced, while the miR-

144-3p inhibitor group showed enhanced proliferation (all P<0.05); the miR-144-3p inhibitor + siRNA-FBN1 group showed no significant change (P>0.05).

Upregulated miR-144-3p or downregulated FBN1 induces apoptosis

Annexin V-APC/PI double staining revealed the apoptotic rates in the six groups (Figure 7). In comparison with the blank and NC groups, the miR-144-3p mimic, siRNA-FBN1 and miR-144-3p inhibitor+siFBN1 groups showed elevated rates. While the miR-144-3p inhibitor group had a reduced rate compared with the NC group (all P<0.05)

Upregulated miR-144-3p or downregulated FBN1 inhibits cell migration

The scratch assay (Figure 8A and 8B) revealed that compared with the blank and NC groups, the miR-144-3p mimic and siRNA-FBN1 groups had lower migration abilities (P<0.05), while the miR-144-3p inhibitor group had markedly enhanced migration ability (P<0.05); cells administered miR-144-3p inhibitor + siRNA-FBN1 inhibitor had unaltered migration ability (P>0.05).

Upregulated miR-144-3p or downregulated FBN1 inhibits cell adhesion

The adhesion assay demonstrated the blank and NC groups were comparable in adhesion ability (P>0.05). In comparison with the blank and NC groups, significantly reduced cell adhesion ability was found in the miR-144-3p mimic and siRNA-FBN1 groups (P<0.05); cells transfected with miR-144-3p inhibitor had significantly elevated adhesion ability (P<0.05), which was unchanged in the miR-144-3p inhibitor + siRNA- FBN1 inhibitor group (P>0.05).

Upregulated miR-144-3p or downregulated FBN1 inhibits cell invasion

Based on transwell assay findings (Figure 9A and 9B), the blank and NC groups had no marked difference (P>0.05). In comparison with the NC and blank groups, the miR-144-3p mimic and siRNA-FBN1 groups had lower cell invasion ability (P<0.05), which was enhanced in cells transfected with miR-144-3p inhibitor (P<0.05), while the miR144-3p inhibitor + siRNA-FBN1 group had unaltered invasion ability (P>0.05).

Discussion

Carotid artery dissection represents an important cause of stroke in young and middle-aged adults. Many risk factors, e.g., hypertension, dyslipidemia, and genetic diseases, all elevate the incidence of arterial dissection. Previous studies related to aortic dissection have focused on genetic susceptibility and genetic impact on the pathogenesis of arterial dissection. [3] The FBN1 gene is the main causative gene of Marfan syndrome, and defects in the latter gene can cause abnormalities in the encoded protein fibrillin-1, resulting in a large group of connective tissue diseases, collectively known as type I fibrillinopathies. Among them, Marfan syndrome (MFS) represents the commonest, and the most important cause of death is cardiovascular accidents, including arterial dissection and aneurysms. Weill-

Marchesani syndrome, acromicric and geleophysic dysplasia, ectopia lentis and scleroderma syndrome are rare. [18]

Our team found in a study performed a few years ago that the fibrillin-1 protein also has an important function in the occurrence and development of cerebral artery dissection, with fibrillin-1 protein level closely related to the severity of the disease. In addition to plasma fibrillin-1 levels being significantly higher in patients with craniocerebral carotid dissection compared with healthy individuals, they are also higher than in patients with ischemic stroke caused by other etiologies; patients with craniocerebral carotid dissection are also characterized by dynamic changes of increased plasma fibrillin-1 in the acute phase and decreased amounts in the chronic phase. [19] In the latter study, we made a new attempt based on the classical method in previous aortic dissections. An animal model of spontaneous carotid dissection was successfully established using mechanical rotation of the carotid artery. The levels of the fibrillin-1 protein were decreased in the dissected tissue after rotation compared with both the non-rotation side and normal carotid tissues.

The fibrillin-1 protein is the main structural component of microfibers, which surround the outermost layer of elastic fibers and constitute the skeleton formed by elastic fibers. This structural composition of microfibers and elastic fibers plays a crucial role in VSMC in billions of stretching and recoil cycles. [20]

Multiple miRNAs are considered to contribute to the pathogenesis of vascular remodeling and aneurysm. [21, 22] The latter findings overtly reveal a role for miRNAs in the development of arterial dissection and aneurysms. In the present study, it was confirmed that miR-144-3p functionally targets FBN1 and negatively regulates the function of VSMC as well as secreted fibrillin-1 protein. The miR-144-3p/FBN1 axis has not been reported previously for its regulatory function. We also firstly examined the biological functional changes of VSMC via regulation of the FBN1 gene by miRNAs in carotid dissection disease. It has been previously shown the miR-29 family of miRNAs contribute to elastin downregulation in adult aorta and are closely related to aortic dissection. Merk et al. further demonstrated miR-29b is important in early aneurysm development in a mouse model of MFS. [23] In the latter work, miR-29b amounts were elevated in thoracic aortic aneurysms of MFS mice, alongside enhanced apoptosis and MMP-2 activity as well as reduced amounts of anti-apoptotic proteins (Mcl-1 and Bcl-2) and elastin. [24] This regulatory mechanism was further confirmed by other studies. In addition, LNA-anti-miR-29b administration suppresses AA development, aortic wall apoptosis and ECM degeneration. [25] However, miR-29 has multiple target genes that directly interact with ≥16 ECM genes, including collagen isoforms (COL1A1, COL1A2, and COL3A1), fibrillin-1 (FBN1) and elastin (ELN), and contribute to extracellular matrix remodeling in many organs. [26–28] These include MMP-2, a gene highly altered in AD. [15] Therefore, the effect of miR-29 in AD pathogenesis should be cautiously interpreted, and multiple possibly associated genes deserve further investigation. In comparison with miR-29, miR-144-3p has far fewer known target genes. Although E26 conversion specific-1, cyclooxygenase-2, adenosine triphosphate-binding cassette transporter and cyclin-dependent kinase inhibitor 2D are documented miR-144-3p's target genes, they have a very limited role in AD development. [12–15] Therefore, it is important to reveal miR144-3p as a regulating miRNA for FBN1.

In the pathogenesis of arterial dissection, vascular remodeling is considered an important link in the development of arterial dissection. [29] Vascular remodeling involves cell growth, death, migration, and extracellular matrix production and degradation. It is not only an adaptive physiological process to maintain vascular homeostasis but also a key pathological link common to many important vascular diseases. VSMC, as the main cellular components of the vascular wall, are critical for maintaining vascular wall tension and structural stability based on their number, distribution and function. [30, 31] The proliferation rate of VSMC in adult blood vessels is very low, and the synthetic function is not active, mainly expressing contractile proteins such as α-SMA, CNN1, SM22α and MYH11. [32] Although the proliferation rate of VSMC in adult blood vessels is different from that of end-differentiated cells of myocardial and skeletal muscle cells, VSMC show certain differentiation ability in case of changes in the vascular environment, regardless of physiological or pathological changes, e.g., a shift to proliferation or synthesis ability to adapt to changes in the internal environment of the body. They also secrete a variety of cytokines such as MCP1, MMPs and ADAMTS, and subsequently induces inflammatory cells to release inflammatory factors; in addition, elastic fibers and collagen fibers are broken, and cell matrix degradation further destroys the structural stability of the vascular wall and participates in the regulation of vascular wall remodeling. [33]

In this work, miR-144-3p upregulation significantly suppressed the proliferative function of VSMC by regulating FBN1. The balance of cell proliferation and apoptosis is an important event in tissue homeostasis. [34] The proliferation of VSMC might have a crucial function in the occurrence and progression of vascular remodeling, while in vasodilatation and hemorrhagic diseases, including aortic dissection and aneurysm, apoptosis of VSMC is more significant in vascular remodeling than cell proliferation in the weak link of the wall. [35] As shown above, miR-144-3p upregulation significantly induced apoptosis in vascular smooth muscle cells, and cell injury and late apoptosis were predominant. Combined with the suppressed effects of miR-144-3p on SMC proliferation in previous studies, it is suggested that in the vascular remodeling of arterial dissection, miR-144-3p upregulation may contribute to the vascular remodeling of the arterial wall by promoting apoptosis in SMC to weaken the arterial medial wall, which in turn affects the occurrence of arterial dissection. Moreover, this study further demonstrated that the expression of the transcription factor Srf was decreased after miR-144-3p overexpression or FBN1 gene knockdown, suggesting that FBN1 dysfunction may also affect the expression of smooth muscle cell’s contractile genes through other mechanisms, e.g., affecting the formation of transcriptional complexes or their binding to SREs.

In addition, the amounts of related extracellular matrix proteins, including elastin and collagen, were also decreased in this work after miR-144-3p upregulation. The expression levels of MMPs, including MMP-2 and MMP-9, which are highly associated with the development of arterial dissection, were elevated in cells transfected with miR-144-3p mimic and siFBN1. Elevated MMPs can further degrade extracellular matrix proteins such as fibrillin-1, produce more fibrillin-1 fragments, forming a vicious cycle and ultimately leading to increased destruction of the vessel wall and poorer stability. [36] It has also been shown that MMPs induce proliferation and migration in VSMC and aggravate vascular wall remodeling. [37]

Conclusions

Overall, this work provides evidence that miR-144-3p promotes smooth muscle cell apoptosis by regulating its target gene FBN1, thereby inhibiting smooth muscle cell invasion, migration, adhesion and proliferation. Smooth muscle cells were also found to transform from contractile to synthetic, with changes in the expression of related extracellular matrix proteins and MMPs. However, there are some major points requiring further analysis, e.g., the detailed mechanism underpinning FBN1 inhibition by miR-144-3p. Therefore, further studies are warranted to identify a safer and more effective approach for targeted therapy and diagnosis.

Abbreviations

CAD: Carotid artery dissection

VSMC: vascular smooth muscle cell

SPF: specific pathogen-free

NC: negative control

HRP: horseradish peroxidase

PAGE: polyacrylamide gel electrophoresis

PVDF: polyvinylidene fluoride

Declarations

Acknowledgments

We thank the Professor Huimin Ren (State Key Laboratory of Medical Neurobiology affiliated to Fudan University) provided technical assistance.

Author's Statements

Funding

None

Author's contributions:

AL: Conceptualization, Methodology, Formal Analysis, Writing Original Draft Preparation;

XK: Writing Review and Editing

YJ: Formal Analysis

XF: Data Curation

WY: Formal Analysis

YL: Formal Analysis

XH: Validation, Project Administration;

QD: Funding Acquisition; Supervision

All authors have read and agreed to the published version of the manuscript.

Conflict of Interest

The authors declare that they have no conflicts of interest.

Data Availability Statement

The original contributions presented in the study are included in the article, further inquiries can be directed to the corresponding author.

Ethical approval

The present study was approved by the Animal Welfare and Ethics Group, Department of Laboratory Animal Science, Fudan University (approval number: 2020 Huashan Hospital JS-425). And the research related to animals' use has been complied with all the relevant national regulations and institutional policies for the care and use of animals.

Informed Consent

Not applicable

References

1. Putaala, J., Metso, A.J., Metso, T.M., et al. Analysis of 1008 consecutive patients aged 15 to 49 with first-ever ischemic stroke: the Helsinki young stroke registry. Stroke 2009;40(4):1195-203.
2. Morello, F., Piler, P., Novak, M.Kruzliak, P. Biomarkers for diagnosis and prognostic stratification of aortic dissection: challenges and perspectives. Biomark Med 2014;8(7):931-41.
3. Mallat, Z., Tedgui, A.Henrion, D. Role of Microvascular Tone and Extracellular Matrix Contraction in the Regulation of Interstitial Fluid: Implications for Aortic Dissection. Arterioscler Thromb Vasc Biol 2016;36(9):1742-7.

4. Segreto, A., Chiusaroli, A., De Salvatore, S.Bizzarri, F. Biomarkers for the diagnosis of aortic dissection. J Card Surg 2014;29(4):507-11.
5. Del Cid, J.S., Reed, N.I., Molnar, K., et al. A disease-associated mutation in fibrillin-1 differentially regulates integrin-mediated cell adhesion. J Biol Chem 2019;294(48):18232-43.
6. Seok, H., Ham, J., Jang, E.S.Chi, S.W. MicroRNA Target Recognition: Insights from Transcriptome-Wide Non-Canonical Interactions. Mol Cells 2016;39(5):375-81.
7. Forman, J.J., Legesse-Miller, A.Coller, H.A. A search for conserved sequences in coding regions reveals that the let-7 microRNA targets Dicer within its coding sequence. Proc Natl Acad Sci U S A 2008;105(39):14879-84.
8. Cao, M.X., Jiang, Y.P., Tang, Y.L.Liang, X.H. The crosstalk between lncRNA and microRNA in cancer metastasis: orchestrating the epithelial-mesenchymal plasticity. Oncotarget 2017;8(7):12472-83.
9. Ivey, K.N., Muth, A., Arnold, J., et al. MicroRNA regulation of cell lineages in mouse and human embryonic stem cells. Cell Stem Cell 2008;2(3):219-29.
10. Li, Q.Gregory, R.I. MicroRNA regulation of stem cell fate. Cell Stem Cell 2008;2(3):195-6.
11. Papagiannakopoulos, T.Kosik, K.S. MicroRNA-124: micromanager of neurogenesis. Cell Stem Cell 2009;4(5):375-6.
12. Zhang, S.Y., Lu, Z.M., Lin, Y.F., et al. miR-144-3p, a tumor suppressive microRNA targeting ETS-1 in laryngeal squamous cell carcinoma. Oncotarget 2016;7(10):11637-50.
13. Shao, Y., Li, P., Zhu, S.T., et al. MiR-26a and miR-144 inhibit proliferation and metastasis of esophageal squamous cell cancer by inhibiting cyclooxygenase-2. Oncotarget 2016;7(12):15173-86.
14. Vega-Badillo, J., Gutiérrez-Vidal, R., Hernández-Pérez, H.A., et al. Hepatic miR-33a/miR-144 and their target gene ABCA1 are associated with steatohepatitis in morbidly obese subjects. Liver Int 2016;36(9):1383-91.
15. Jiang, W., Zhang, Z., Yang, H., et al. The Involvement of miR-29b-3p in Arterial Calcification by Targeting Matrix Metalloproteinase-2. Biomed Res Int 2017;2017:6713606.
16. Sato, F., Seino-Sudo, R., Okada, M., et al. Lysyl Oxidase Enhances the Deposition of Tropoelastin through the Catalysis of Tropoelastin Molecules on the Cell Surface. Biol Pharm Bull 2017;40(10):1646-53.
17. Lewis, B.P., Burge, C.B.Bartel, D.P. Conserved seed pairing, often flanked by adenosines, indicates that thousands of human genes are microRNA targets. Cell 2005;120(1):15-20.
18. Sakai, L.Y., Keene, D.R., Renard, M.De Backer, J. FBN1: The disease-causing gene for Marfan syndrome and other genetic disorders. Gene 2016;591(1):279-91.
19. Zhu, Z., Tang, W., Ge, L., Han, X.Dong, Q. The value of plasma fibrillin-1 level in patients with spontaneous cerebral artery dissection. Neurology 2018;90(9):e732-e7.
20. Helbig, G.Krzemień, S. Clinical significance of elastin turnover–focus on diseases affecting elastic fibres. Wiad Lek 2004;57(7-8):360-3.

21. Fu, X.M., Zhou, Y.Z., Cheng, Z., Liao, X.B.Zhou, X.M. MicroRNAs: Novel Players in Aortic Aneurysm. Biomed Res Int 2015;2015:831641.
22. Ott, C.E., Grünhagen, J., Jäger, M., et al. MicroRNAs differentially expressed in postnatal aortic development downregulate elastin via 3' UTR and coding-sequence binding sites. PLoS One 2011;6(1):e16250.
23. Merk, D.R., Chin, J.T., Dake, B.A., et al. miR-29b participates in early aneurysm development in Marfan syndrome. Circ Res 2012;110(2):312-24.
24. Chuang, T.D., Pearce, W.J.Khorram, O. miR-29c induction contributes to downregulation of vascular extracellular matrix proteins by glucocorticoids. Am J Physiol Cell Physiol 2015;309(2):C117-25.
25. Okamura, H., Emrich, F., Trojan, J., et al. Long-term miR-29b suppression reduces aneurysm formation in a Marfan mouse model. Physiol Rep 2017;5(8).
26. Sudo, R., Sato, F., Azechi, T.Wachi, H. MiR-29-mediated elastin down-regulation contributes to inorganic phosphorus-induced osteoblastic differentiation in vascular smooth muscle cells. Genes Cells 2015;20(12):1077-87.
27. van Rooij, E., Sutherland, L.B., Thatcher, J.E., et al. Dysregulation of microRNAs after myocardial infarction reveals a role of miR-29 in cardiac fibrosis. Proc Natl Acad Sci U S A 2008;105(35):13027-32.
28. Boon, R.A., Seeger, T., Heydt, S., et al. MicroRNA-29 in aortic dilation: implications for aneurysm formation. Circ Res 2011;109(10):1115-9.
29. Jones, J.A., Beck, C., Barbour, J.R., et al. Alterations in aortic cellular constituents during thoracic aortic aneurysm development: myofibroblast-mediated vascular remodeling. Am J Pathol 2009;175(4):1746-56.
30. Kwon, S.T., Rectenwald, J.E.Baek, S. Intrasac pressure changes and vascular remodeling after endovascular repair of abdominal aortic aneurysms: review and biomechanical model simulation. J Biomech Eng 2011;133(1):011011.
31. Haller, H., Lindschau, C., Quass, P., Distler, A.Luft, F.C. Differentiation of vascular smooth muscle cells and the regulation of protein kinase C-alpha. Circ Res 1995;76(1):21-9.
32. Wu, D., Shen, Y.H., Russell, L., Coselli, J.S.LeMaire, S.A. Molecular mechanisms of thoracic aortic dissection. J Surg Res 2013;184(2):907-24.
33. Owens, G.K., Kumar, M.S.Wamhoff, B.R. Molecular regulation of vascular smooth muscle cell differentiation in development and disease. Physiol Rev 2004;84(3):767-801.
34. Simón, R., Aparicio, R., Housden, B.E., Bray, S.Busturia, A. Drosophila p53 controls Notch expression and balances apoptosis and proliferation. Apoptosis 2014;19(10):1430-43.
35. Ping, S., Li, Y., Liu, S., et al. Simultaneous Increases in Proliferation and Apoptosis of Vascular Smooth Muscle Cells Accelerate Diabetic Mouse Venous Atherosclerosis. PLoS One 2015;10(10):e0141375.

36. Grond, G.C., Pjontek, R., Aksay, S.S., et al. Spontaneous arterial dissection: phenotype and molecular pathogenesis. Cell Mol Life Sci 2010;67(11):1799-815.
37. Zhang, H., Wang, Z.W., Wu, H.B., et al. Transforming growth factor-β1 induces matrix metalloproteinase-9 expression in rat vascular smooth muscle cells via ROS-dependent ERK-NF-κB pathways. Mol Cell Biochem 2013;375(1-2):11-21.

Tables

Table 1. Primers for RT-qPCR

Gene	Sequence(5’to3’)
miR-144-3p	Forward: CGCGCGCTACAGTATAGATG
	Reverse: CTCCGAGACAGCCCCATCCA
FBN1	Forward: ATCACCATCTTCCAGGAG
	Reverse: CTCCGAGACAGCCCCATCCA
MYH11	Forward: ATCACCATCTTCCAGGAG
	Reverse: CTCCGAGACAGCCCCATCCA
CNN1	Forward: AGCGGAGATTTGAGCCTGAG
	Reverse: CAAAGATCTGCCGCTTGGTG
ACTA2	Forward: GCGTGGCTATTCCTTCGTTA
	Reverse: ATGAAGGATGGCTGGAACAG
MMP2	Forward: GGTGTGCAACCACAACCAAC
	Reverse: TGTAGGCGTGGGTCCAGTA
MMP9	Forward: GCCGGGAACGTATCTGGAAA
	Reverse: GGTTGTGGAAACTCACACGC
ELN	Forward: ATCACCATCTTCCAGGAG
	Reverse: CTCCGAGACAGCCCCATCCA
COL1A1	Forward: ATCACCATCTTCCAGGAG
	Reverse: CTCCGAGACAGCCCCATCCA
SRF	Forward: GCTTCACTCTCATGCCTGGT
	Reverse: TGCATGGGGACTAGGGTACA
GAPDH	Forward: ATCACCATCTTCCAGGAG
	Reverse: CTCCGAGACAGCCCCATCCA
U6	Forward: CGCTTCGGCAGCACATATAC

Reverse: TTCACGAATTTGCGTGTCAT

miR-144-3p, microRNA-144-3p; FBN1, fibrillin-1; MYH11, smooth muscle myosin heavy chain 11; CNN1 calponin1; ACTA2, smooth muscle-actin; MMP, matrix metalloproteinase; ELN, elastin; COL1A1, collagen, type I, alpha 1; GAPDH, glyceraldehyde-3-phosphate dehydrogenase; RT-qPCR, reverse transcription quantitative polymerase chain reaction.

Figures

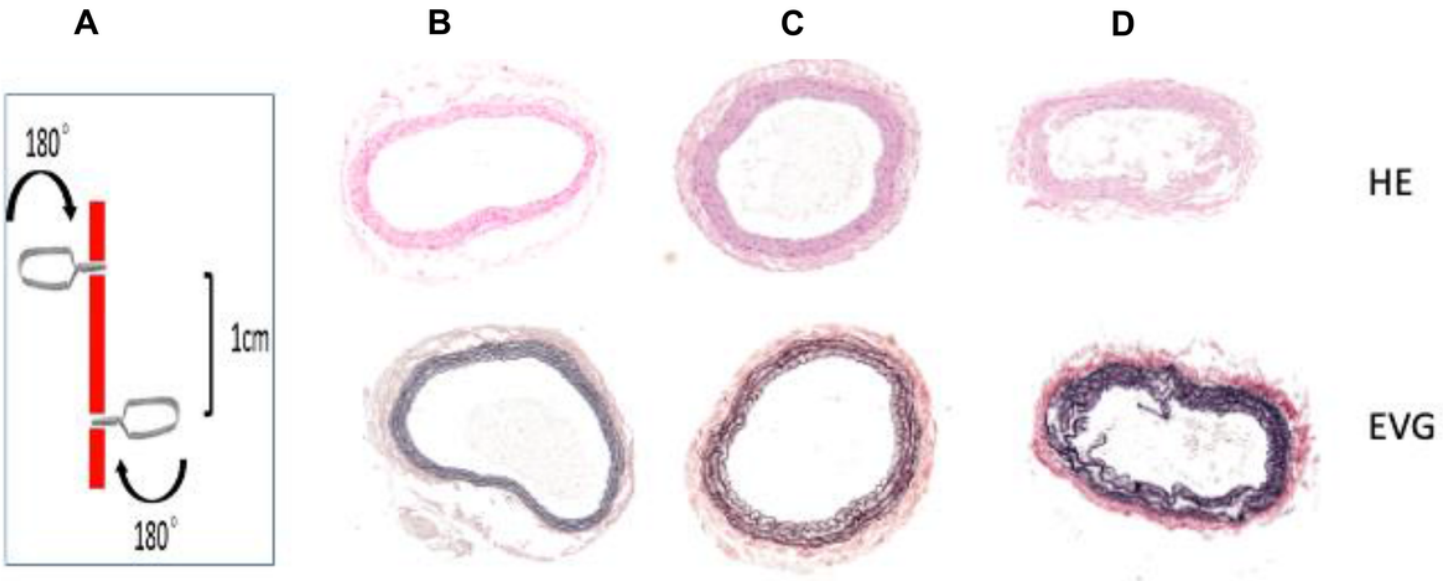

Figure 1

Pathological changes of normal carotid artery wall and carotid artery wall of arterial dissection by H&E staining and EVG elastic fiber staining. (A) A spontaneous arterial dissection model was established by carotid mechanical clip rotation. (B) Staining of normal arterial wall. (20 ×) (C)Staining of the carotid artery tissue of the non-rotation side of model animals. (20 ×) (D) Staining of the carotid artery tissue of the rotation side of model animals. (20 ×).

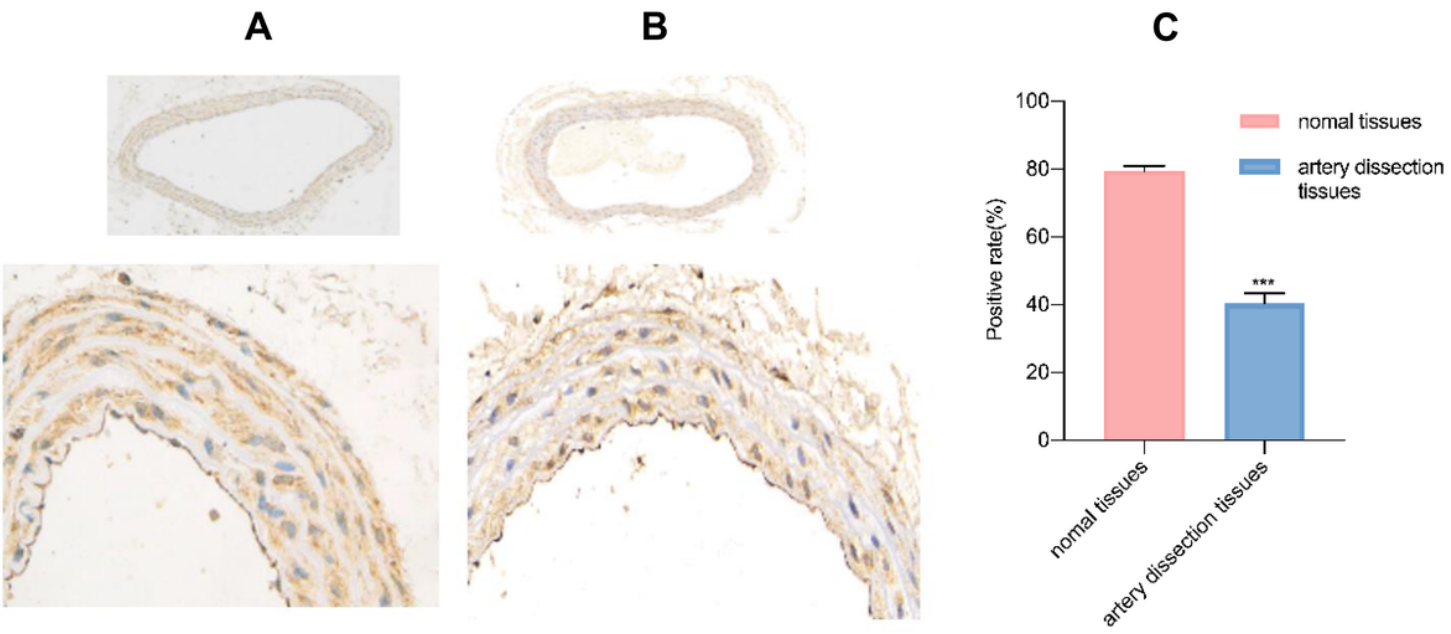

Figure 2

Fibrillin-1 protein expression is decreased in arterial dissection tissue compared with normal carotid wall tissue. (A) Immunohistochemical detection of the fibrillin-1 protein in normal carotid artery wall tissue (40 ×) (B) Immunohistochemical detection of the fibrillin-1 protein in the arterial dissection tissue (40 ×). (C) Positivity rates of fibrillin-1 in normal carotid artery wall and arterial dissection tissue. * P<0.5 versus normal tissue. Data are mean±standard deviation, and were compared by the t-test. Assays were carried out thrice.

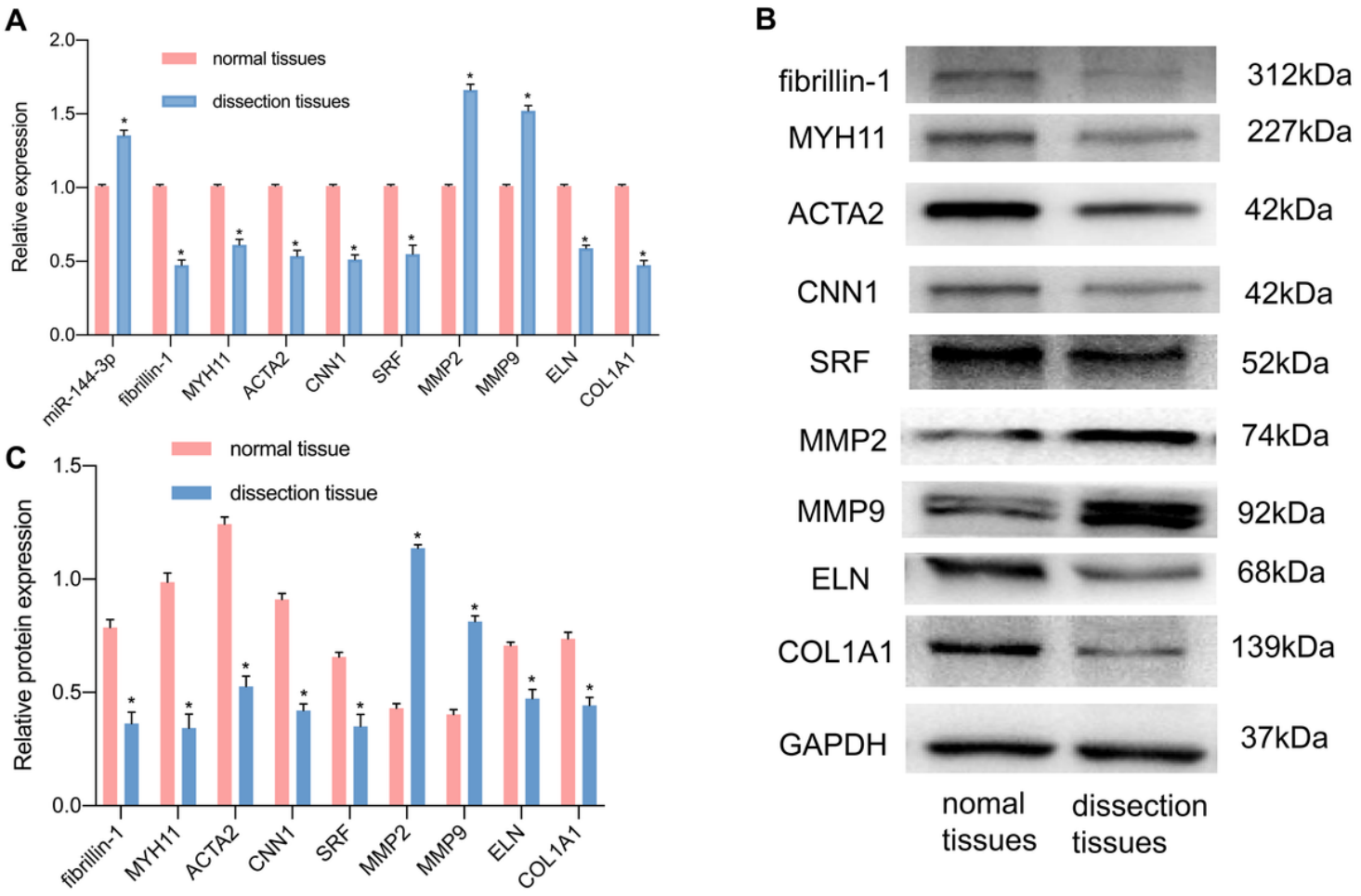

Figure 3

Expression of miR-144-3p, FBN1 gene and VSMC contraction genes in arterial dissection tissues. (A) MiR-144-3p amounts and FBN1, MYH11, ACTA2, CNN1, SRF, MMP2, MMP9, ELN and COL1A1 mRNA amounts. (B)Gray values of FBN1, MYH11,ACTA2, CNN1, SRF, MMP2, MMP9, ELN and COL1A1 protein bands. (C) FBN1, MYH11, ACTA2, CNN1, SRF, MMP2, MMP9, ELN and COL1A1 protein amounts. *P<0.05 compared with the normal group. Data are mean ± standard deviation (SD); the t-test was performed to compare groups in experiments repeated thrice.

A

	Predicted Consequential Pairing of Target Region (Top)And Mirna (Bottom)	Site Type	Context++ Score	Context++ Score Percentile	Weighted Context++ Score	Conserved Branch Lengh	Pct
position 2611-2617 of FBN1 3'UTR hsa-miR-144-3p	5'…AUAUUGCCAUUACAAAUACUGUU 3' UCAUGUAGUAGAUAUGACAU	7mer-m8	-0.15	89	-0.05	2.958	0.30

B

	Predicted Consequential Pairing of Target Region (Top)And Mirna (Bottom)	Site Type	Context++ Score	Context++ Score Percentile	Weighted Context++ Score	Conserved Branch Lengh	Pct
position 2585-2591 of FBN1 3'UTR rno-miR-144-3p	5'…AUGCUGCCAUUACAAAUACUGUU 3' UCAUGUAGUAGAUAUGACAU	7mer-m8	-0.15	89	-0.05	2.958	0.30

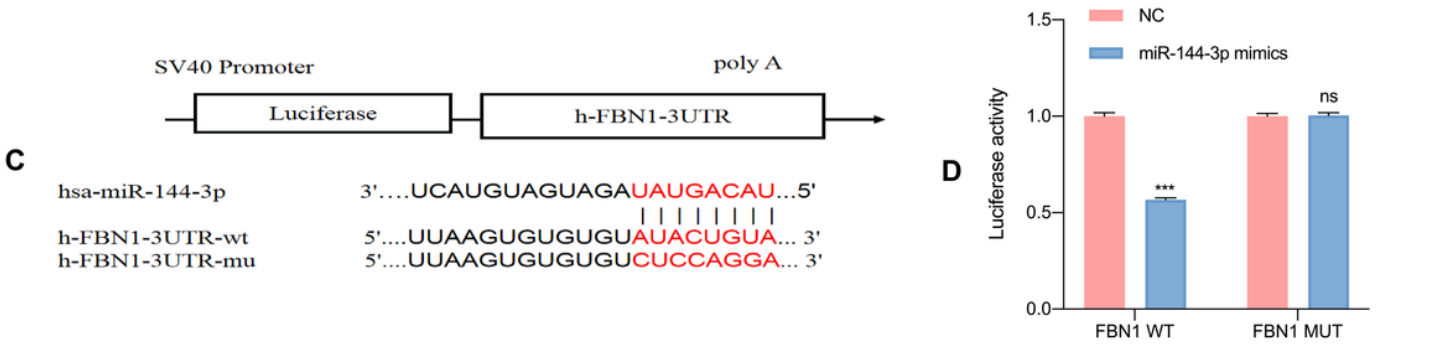

Figure 4

FBN1 is the target gene of miR-144-3p (A, B) Bioinformatics analysis revealing miR-144-3p's binding site at the 3'-UTR of human FBN1 mRNA ranged from 2611 to 2617 base pairs (A), versus from 2585 to 2591 base pairs in rats (B). (C) Schematic representation of hsa-miR-144-3p interaction h-FBN1-3'UTR target sites (D) Dual-luciferase reporter assay of hsa-miR-144-3p interaction with h-FBN1-3'UTR

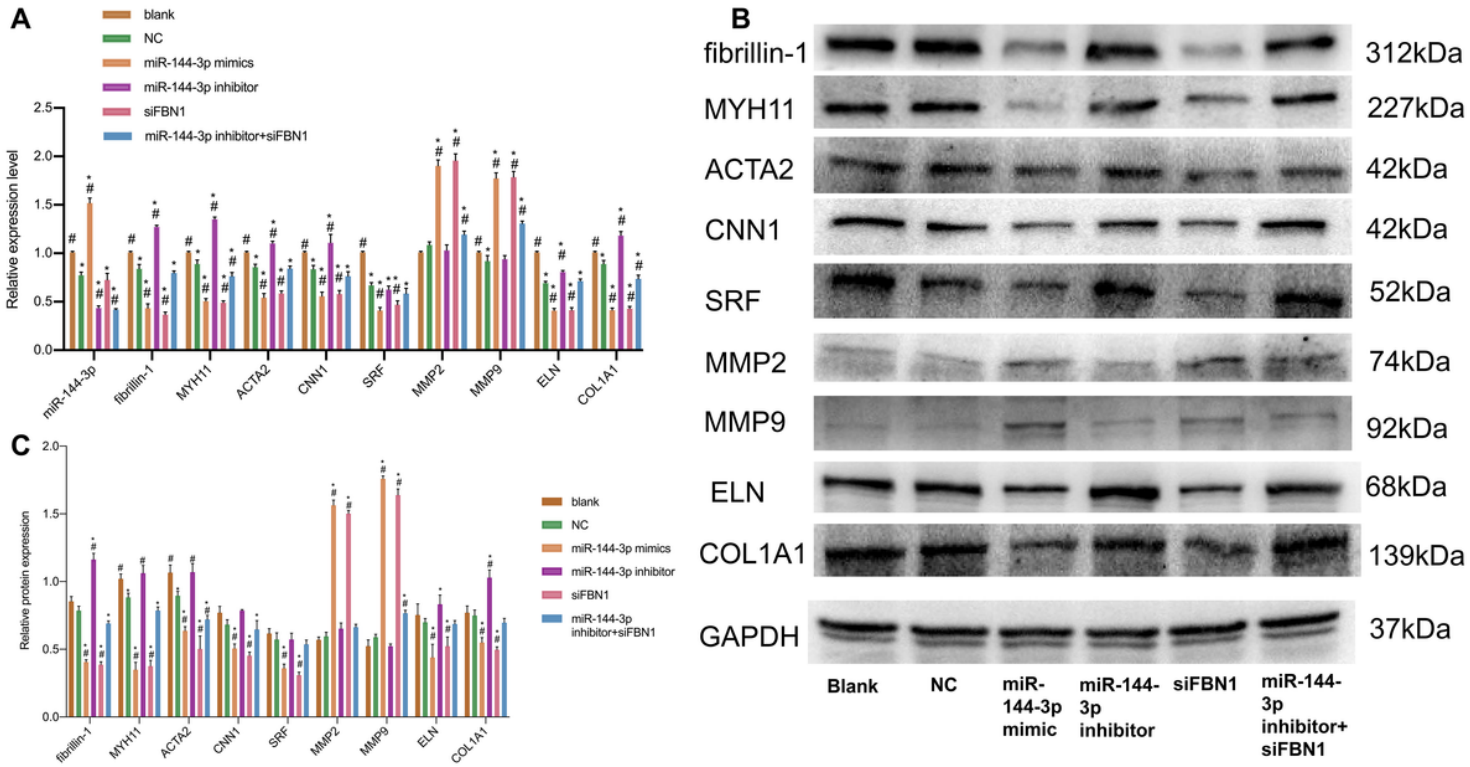

Figure 5

MiR-144-3p's effects on extracellular matrix and vascular smooth muscle phenotype genes. (A) The mRNA expression levels of FBN1, MYH11, CNN1, ACTA2, COL1A1, ELN, MMP2 and MMP9 after treatment with miR-144-3p mimic, miR-144-3p inhibitor, siRNA-FBN1 and miR-144-3p inhibitor + siRNA-FBN1 are shown. (B) Protein band gray values for FBN1, MYH11, CNN1, ACTA2, COL1A1, ELN, MMP2 and MMP9 after treatment with miR-144-3p mimic, miR-144-3p inhibitor, siRNA-FBN1 and miR-144-3p inhibitor + siRNA-FBN1. (C) FBN1, MYH11, CNN1, ACTA2, COL1A1, ELN, MMP2 and MMP9 protein amounts after treatment with miR-144-3p mimic, miR-144-3p inhibitor, siRNA-FBN1 and miR-144-3p inhibitor + siRNA-FBN1.

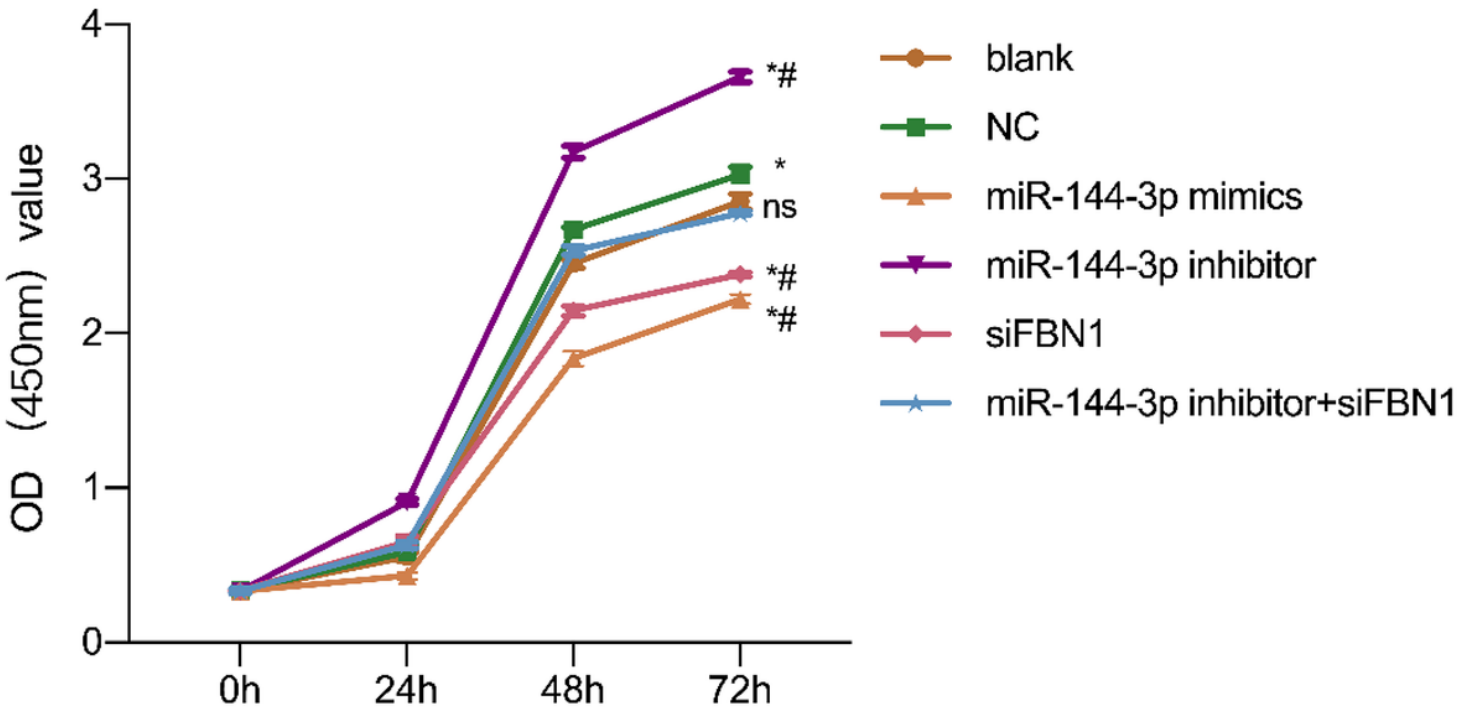

Figure 6

Overexpressed miR-144-3p or siRNA-FBN1 decreased SMC proliferation. *P<0.05 for each group versus blank group. #P<0.05 versus NC group. Data are mean±standard deviation; repeated measures ANOVA was performed for comparisons, in experiments repeated thrice. NC, negative control; OD, optical density

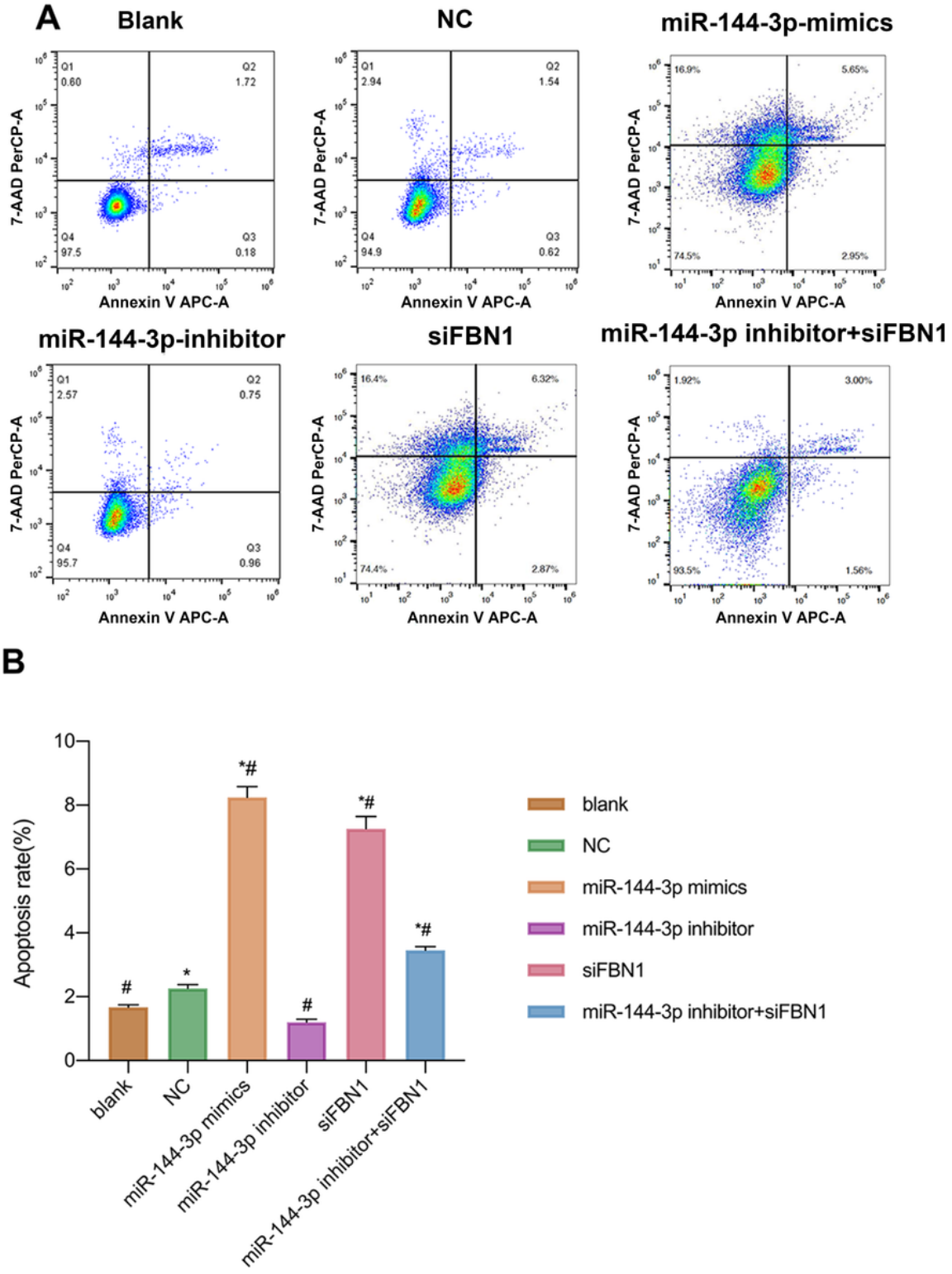

Figure 7

Upregulated miR-144-3p or FBN1 knockdown induces A7R5 SMC apoptosis. (A) Flow cytometry profiles demonstrating A7R5 SMC apoptosis.(B)Analysis of apoptotic rates in A7R5 SMC cells upon treatment with miR-144-3p mimic, miR-144-3p inhibitor, siRNA-FBN1 and miR-144-3p inhibitor + siRNA-FBN1. *P<0.05 vs blank group; #P<0.05 vs NC group.

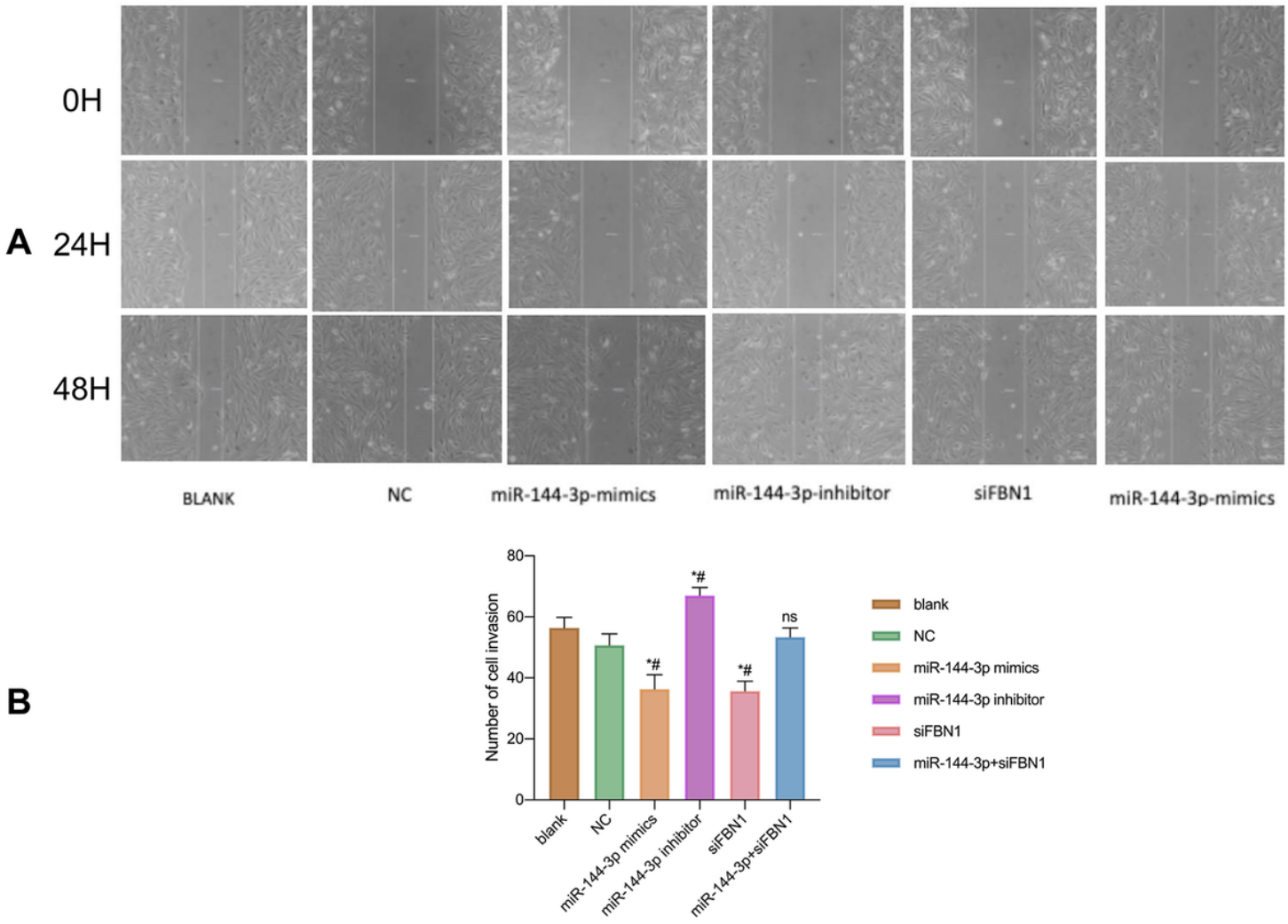

Figure 8

Overexpressed miR-144-3p or siRNA-FBN1 inhibits cell migration. (A) Scratch wound healing in SMC cells after transfection with miR-144-3p mimic, miR-144-3p inhibitor, siRNA-FBN1 and miR-144-3p inhibitor + siRNA-FBN1.(B)Cell migration distances are shown. *P<0.05 versus blank NC group;#P<0.05 vs NC group. Data are mean±standard deviation; one-way ANOVA was carried out to compare multiple groups, in assays performed thrice. ANOVA, analysis of variance

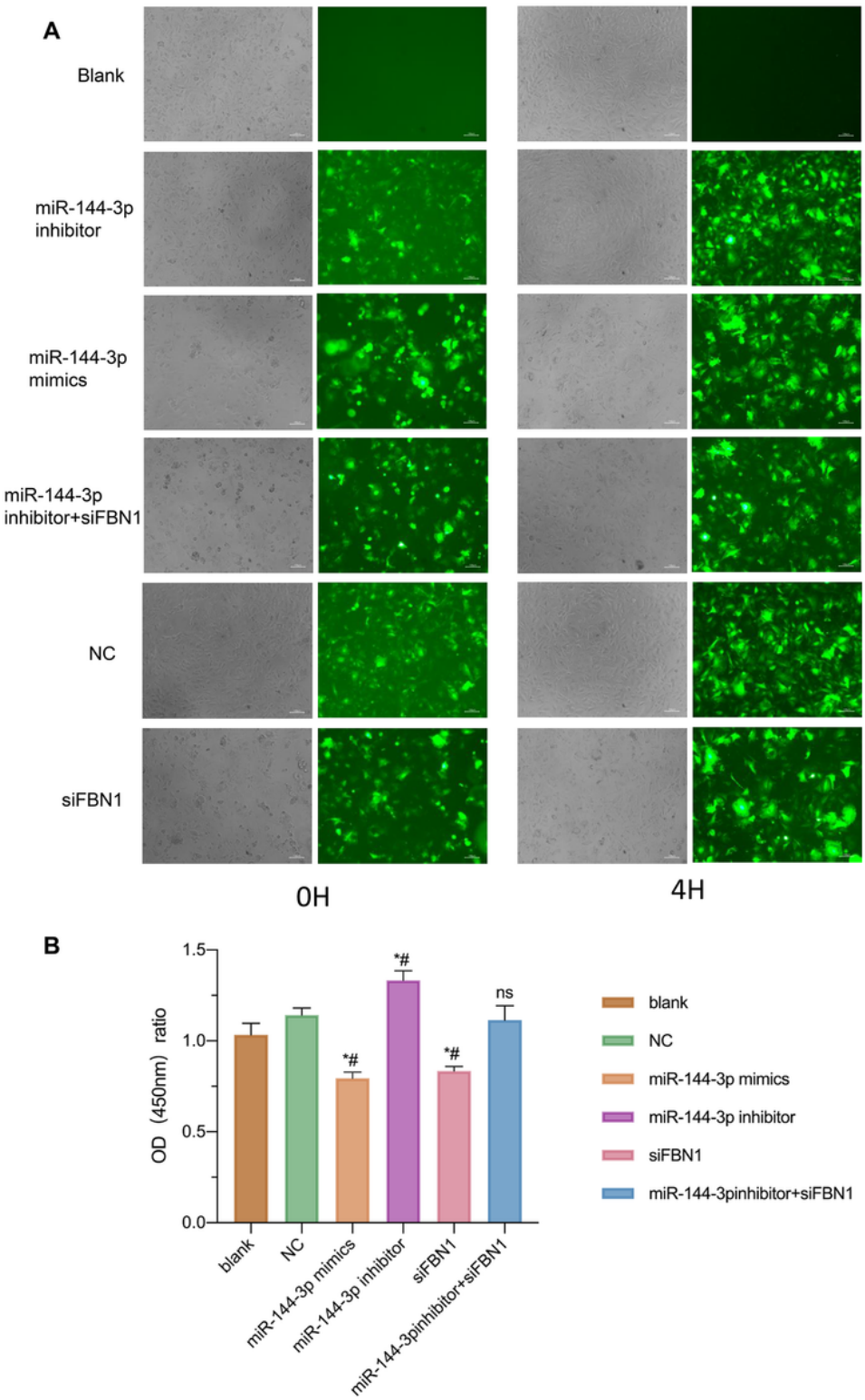

Figure 9

Overexpressed miR-144-3p or siRNA-FBN1 inhibits cell adhesion. (A) Adhesion conditions in A7R5 SMC after transfection with miR-144-3p mimic, miR-144-3p inhibitor, siRNA-FBN1 and miR-144-3p inhibitor + siRNA-FBN1. (B) Quantitation of A. *P<0.05 versus blank group;#P<0.05 vs NC group. Data are mean±standard deviation; one-way ANOVA was carried out to compare multiple groups, in assays performed thrice. ANOVA, analysis of variance.

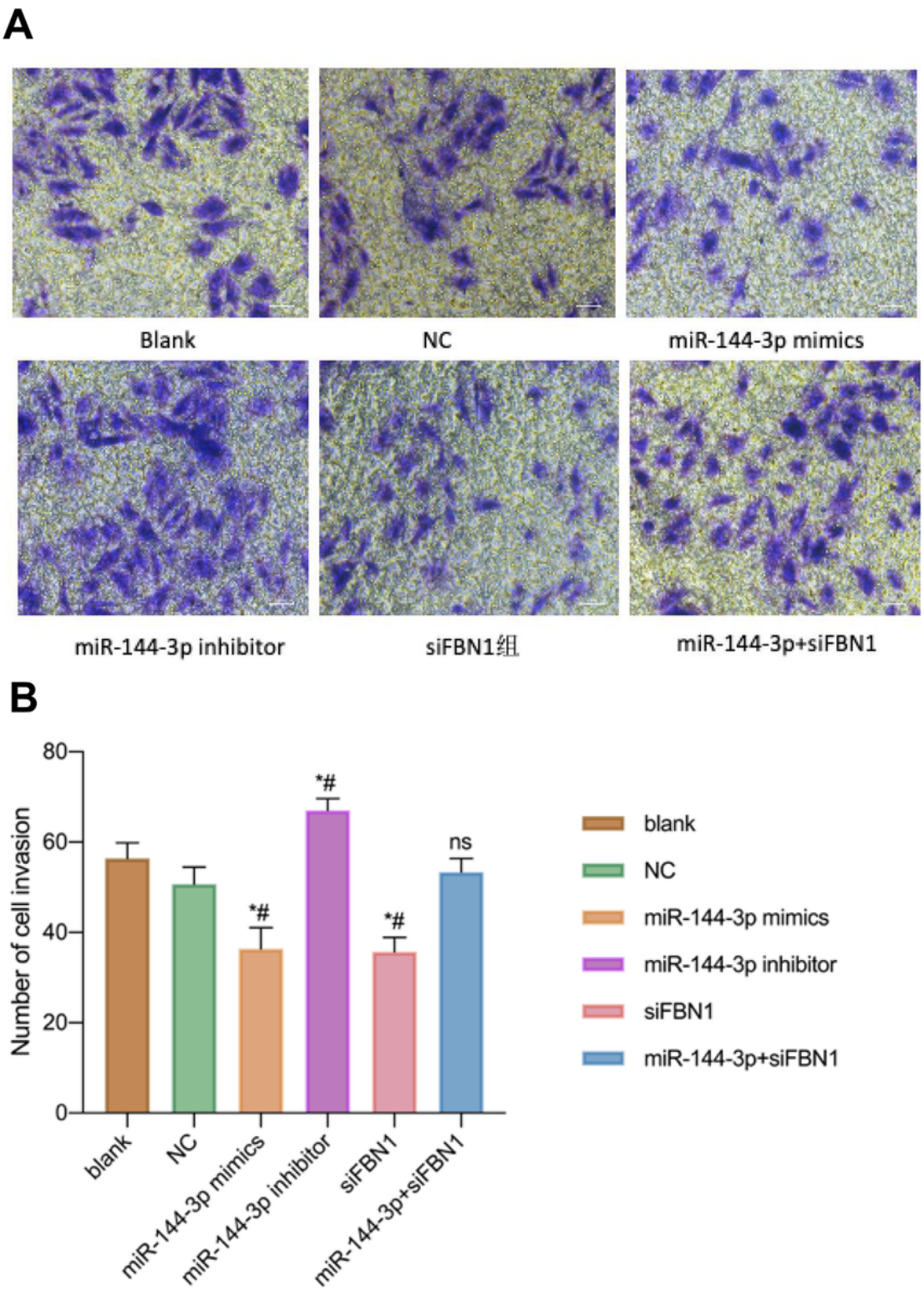

Figure 10

Overexpressed miR-144-3p or siRNA-FBN1 suppresses cell invasion. (A) Cells that passed through the bottom chamber were underwent crystal violet staining (× 100). (B) Quantitation of A. *P<0.05 versus blank group;#P<0.05 vs NC group. Data are mean±standard deviation; one-way ANOVA was carried out to compare multiple groups, in assays performed thrice. ANOVA, analysis of variance.

Supplementary Files

This is a list of supplementary files associated with this preprint. Click to download.

- AuthorChecklistFull.pdf